Hierarchical theories of structures based on Legendre polynomial expansions with finite element applications

Hierarchical theories of structures based on Legendre polynomial expansions with finite element applications

E. Carrera*, A.G. de Miguel †, A. Pagani‡

Department of Mechanical and Aerospace Engineering, Politecnico di Torino,
Corso Duca degli Abruzzi 24, 10129 Torino, Italy.

Author for correspondence:
E. Carrera, Professor of Aerospace Structures and Aeroelasticity,
Department of Mechanical and Aerospace Engineering,
Politecnico di Torino,
Corso Duca degli Abruzzi 24,
10129 Torino, Italy,
tel: +39 011 090 6836,
fax: +39 011 090 6899,
e-mail: erasmo.carrera@polito.it

*Professor of Aerospace Structures and Aeroelasticity, e-mail: erasmo.carrera@polito.it
†Marie Curie PhD Student, e-mail: alberto.garcia@polito.it
‡Assistant professor, e-mail: alfonso.pagani@polito.it

Abstract

This paper discusses classical and refined beam and plate theories based on the Carrera Unified Formulation (CUF). Attention is focussed on (but not limited to) a new refined beam element with enhanced kinematics based on Legendre polynomial expansions of the primary mechanical variables. By employing CUF, the governing equations and the related finite element arrays are written in a hierarchical, compact and general manner. Readily, these characteristics are used to arbitrarily tune the finite element model at the cross-sectional level, by locally enriching the theory kinematics up to the desired accuracy. The uncompromising accuracy of the present beam model is demonstrated by considering various numerical examples, including solid and thin-walled beams with open and close cross-sections as well as plate structures. The results are compared with those from classical and already established refined CUF models. Eventually, three-dimensional elasticity solutions by the commercial tool MSC Nastran are also given to underline the high accuracy of the present methodology. The numerical efficiency and the capabilities of the Legendre-based CUF beam models to deal with complex structures with no geometrical approximations result clear from the analyses conducted.

Keywords: Refined beam theories, Refined plate theories, Finite elements, Carrera Unified Formulation, Hierarchical Legendre expansion, Thin-walled beam.

1 Introduction

Beam theories have become an important tool for the analysis of structural problems. One-dimensional (1D) models, or beam models, are used mainly for the analysis of slender structural bodies, commonly employed in several construction fields such as aerospace or civil engineering. These models result very effective because of their low computational costs in comparison with 2D and 3D ones. Classical beam theories, introduced by Euler [1] and then by Timoshenko [2], have several limitations because they have a-priori fixed kinematics and are only suitable for a limited class of problems (e.g., long beams subjected to bending, homogeneous structures, etc.). In order to take into account other effects, such as torsion, warping or cross-sectional deformations, more sophisticated kinematics shall be employed.

Many refined beam models have been developed to enhance the capabilities of the classical theories in order to describe higher-order effects while keeping the computational costs as low as possible. A discussion of various theories for plates and beams was carried out by Kapania and Raciti [3] [4], who laid emphasis on shear effects, vibrations and wave propagation. A locking-free finite element model based on the exact solution of the Timoshenko beam theory was developed by Reddy [5]. Vinayak et al. [6] discussed beam elements based on higher-order theories. In this work, particular attention was given to flexure of beams and plates, approached through finite element formulations developed starting from the Lo-Christensen-Wo theory. An approximation of shear stresses in prismatic beams was provided by Gruttmann et al. [7] by considering the Saint-Venànt torsion and bending. The same model was then applied to the study of thin-walled beams by Gruttmann and Wagner [8]. Petrolito [9] studied the effects of higher-order shear deformation theory on the element stiffness matrix in comparison with classic beam theories. The stiffness terms were obtained by Eisenberger [10] directly from the governing differential equations that describe the deformations of the cross-section for higher-order theories. The Generalized Beam Theory (GBT) was employed by Silvestre [11] and Rendek and Baláž [12]. The former used GBT for the analysis of the elastic buckling behaviour of circular hollow-section beams, whereas the latter work was focused on the study of prismatic thin-walled steel beams providing also a comparison with experimental results. De Miranda et al. [13] presented a recovery of classical and non-classical beam theories within the framework of the GBT, introducing a new formulation with shear deformation. An analytical deflection trial function was used to describe the modes for dynamic analysis by Cao et al. [14], showing that the accuracy of the analytical trial function is almost identical to that of dynamic stiffness matrix method, whose applications in engineering are limited. Another work on the beam problem was recently carried out by Genoese et al. [15]. In this study, the authors used a mixed formulation based on the HellingerReissner principle, in which the kinematics are constituted by a rigid section with non uniform out-of-plane warping and the stresses are described by means of the Saint-Venànt solution.

It is clear that many different refined beam theories have been developed in the past years to provide more sophisticated and efficient models to solve one-dimensional structural prob-

lems. The present work presents a 1D higher-order beam model based on the Carrera Unified Formulation (CUF), which has been developed by Carrera and his co-workers in the past few years. CUF was devised to overcome the limitations of the classical models by describing the kinematics of structural theories and related governing equations in a hierarchical, unified and compact manner. Initially, Carrera [16, 17] proposed CUF for two-dimensional (2D) analyses. Subsequently, various authors employed CUF to formulate plate and shell theories for structural and multi-field problems, see for example [18, 19, 20, 21]. The extension of CUF to beam modelling was carried out by Carrera and Giunta [22], who adopted hierarchical N-order approximations of the primary mechanical variables based on Mclaurin polynomial series. This class of 1D CUF models, which are known as TE (Taylor Expansion) models in the literature, have been used in various works (see for example [23, 24, 25, 26, 27]). A review of the most significant beam models developed within the framework of CUF was recently done by Carrera et al. [28]

By employing Lagrange polynomials to develop beam theories, a new CUF model was introduced by Carrera and Petrolo [29]. In that paper, the enhanced capabilities of the LE (Lagrange Expansion) CUF models were discussed and particular attention was focused on the capability of LE to deal with 3D-elasticity solutions of simple to complex structures with very low computational efforts. In recent works, LE was employed and extended to deal with the analysis of multi-component structures [30, 31, 32].

In this paper, a new class of 1D CUF beam models is devised by adopting Legendre-like polynomial expansions to develop theories of structures. The one-dimensional Hierarchical Legendre Expansion models (hereinafter referred to as HLE models) are, in fact, formulated by expressing the 3D displacement field as a Legendre-based expansion of the generalized displacements along the beam axis. As it will be clear later in this manuscript, HLE combines the main advantages of TE (e.g., the hierarchy of the higher-order terms) and LE (e.g., exact geometrical description of the beam physical surfaces). The Legendre polynomials that are utilized in this work are not new in solid mechanics. Those polynomials were widely exploited by Babŭska and his co-authors to develop the p-version of Finite Element Method (FEM). In [33], for example, they underlined the high rates of convergence for properly designed meshes, relying on the possibility of increasing the p-order of the polynomial approximation up to some required level of precision. Szabó et al. [34] used a Legendre-type basis to develop the p-FEM for one-dimensional, quadrilateral and hexahedral elements. A wide variety of linear and non-linear examples was also provided, showing that for well defined meshes, the rates of convergence are exponential. The characteristics of a finite element space were established by Szabó and Babŭska in [35]. Lagrange-type and hierarchial shape functions were also described and then applied to the definition of many types of element's geometries in the same work. However, it is important to underline that the main novelty of the present work is that Legendre polynomials are used to develop theories of structures and not numerical methods.

The structure of the paper is the following: a brief introduction to classical beam and plate theories is given in Section 2, followed by the description of refined models based on

the CUF (Section 3). Here, considerable attention is given to HLE. The constitutive law and the geometrical relations are provided in Section 4.1. The introduction to FEM and the development of the stiffness matrix by means of the principle of virtual displacements are included in Sections 4.2 and 4.3. The numerical results obtained from the different cases of study considered are included in Section 5, whereas the conclusions extracted from this work can be found in Section 6.

2 From classic to refined kinematics

2.1 Beam theories

Classical beam models have demonstrated to be a useful tool for the analysis of slender isotropic structures on bending-dominant cases. The most well-known beam theories are the Euler-Bernoulli Beam Theory [1] (hereinafter referred to as EBBT) and the Timoshenko Beam Theory [2] (hereinafter referred to as TBT). Although they perform well within their limiting hypotheses, they lack in representing correctly non-classical effects such as the transverse shear stresses or the rotatory inertia. The EBBT does not account for them, whereas the TBT assumes a uniform shear distribution along the cross-section.

Let us consider a generic beam structure whose longitudinal axis, with respect to a Cartesian coordinate system, lays on the coordinate y, being its cross-section defined in the xz-plane. The kinematic field of EBBT according to this coordinate system reads:

$$\begin{aligned} u_x(x,y,z) =& u_{x_1}(y) \\ u_y(x,y,z) =& u_{y_1}(y) - x\frac{\partial u_{x_1}(y)}{\partial y} - z\frac{\partial u_{z_1}(y)}{\partial y} \\ u_z(x,y,z) =& u_{z_1}(y) \end{aligned} \tag{1}$$

where u_x, u_y and u_z are the components of the 3D displacement field vector and u_{x_1}, u_{y_1} and u_{z_1} represent the displacements of the beam axis. According to Eq. (1), the cross-section always remains rigid, plane and normal to the deformed axis of the beam. As a consequence, the EEBT does not account for transverse shear stresses, which, in many cases, play a major role in the behaviour of the structure. The TBT overcomes this fact by relaxing the assumption of the orthogonality of the cross-section to the deformed axis, resulting in the following kinematics:

$$\begin{aligned} u_x(x,y,z) =& u_{x_1}(y) \\ u_y(x,y,z) =& u_{y_1}(y) + x\phi_z(y) - z\phi_x(y) \\ u_z(x,y,z) =& u_{z_1}(y) \end{aligned} \tag{2}$$

where the number of unknowns have been increased by two with respect to the EBBT kinematics: the rotations ϕ_z around the z-axis and ϕ_x around the x-axis.

When it comes to short, thin-walled, non-homogeneous and/or open section beams, the classic models cannot provide proper results and more sophisticated theories are required. One

problem of TBT is that it does not satisfy the stress-free condition at the section borders, since it assumes a constant distribution of the shear stresses on the cross-section; i.e., $\sigma_{yz} = \sigma_{yz}(y)$ and $\sigma_{xy} = \sigma_{xy}(y)$ are independent of the cross-section coordinates x and z. A possible solution can be to use a third order displacement field that allows the shear stress distribution to return to zero at the borders (see the Vlasov beam theory [36]):

$$\begin{aligned} u_x(x,y,z) =& u_{x_1}(y) \\ u_y(x,y,z) =& u_{y_1}(y) + f_1(x)\phi_z(y) + g_1(x)\frac{\partial u_{x_1}(y)}{\partial y} + f_2(z)\phi_x(y) + g_2(z)\frac{\partial u_{z_1}(y)}{\partial y} \\ u_z(x,y,z) =& u_{z_1}(y) \end{aligned} \tag{3}$$

where f_1, g_1, f_2 and g_2 are cubic functions of the x and z-coordinates. According to this latter kinematics, the transverse shear stresses follow a quadratic distribution on the cross-section and the homogeneous conditions are fulfilled, while the number of degrees of freedom remains the same as for the TBT. Moreover, the Vlasov model overcomes the hypothesis of constant shear by assuming a refined approximation of the mechanical variables. A step further can be to include the effects due to the application of torsional moments. This can be achieved by adding a rigid rotation of the cross-section around the y-axis, resulting in the following kinematic field:

$$\begin{aligned} u_x(x,y,z) =& u_{x_1}(y) + z\phi_y(y) \\ u_y(x,y,z) =& u_{y_1}(y) + f_1(x)\phi_z(y) + g_1(x)\frac{\partial u_{x_1}(y)}{\partial y} + f_2(z)\phi_x(y) + g_2(z)\frac{\partial u_{z_1}(y)}{\partial y} \\ u_z(x,y,z) =& u_{z_1}(y) - x\phi_y(y) \end{aligned} \tag{4}$$

being the new term ϕ_y the rotation around the beam axis. Although each model presented in this section improves the performance of the former ones, higher-order effects such as the second-order cross-sectional deformations or shear stress distributions on thin-walled beams require the use of even more sophisticated theories in which the kinematic field is enriched appropriately (see [28]).

2.2 Plate theories

From the conceptual but not chronological standpoint, plate theories have followed mostly the same evolution as beam theories during their earlier developments. The classical plate model is based on the well-known Kirchoff-Love hypotheses [37]. Analogous to EBBT, the classical plate model assumes that straight lines normal to the mid-surface remain straight and normal to the mid-surface after deformation. Moreover, the thickness of the plate does not change during the deformation. Thus, by considering the mid-plane of the plate laying in the xy-plane, the kinematic field of the Kirchoff-Love plate model can be formulated as

$$\begin{aligned} u_x(x,y,z) =& u_{x_1}(x,y) - z\frac{\partial u_{z_1}(x,y)}{\partial x} \\ u_y(x,y,z) =& u_{y_1}(x,y) - z\frac{\partial u_{z_1}(x,y)}{\partial y} \\ u_z(x,y,z) =& u_{z_1}(x,y) \end{aligned} \tag{5}$$

where u_{x_1}, u_{y_1} and u_{z_1} are the displacements of the mid-plane. $\phi_y(x,y) = -\frac{\partial u_{z_1}}{\partial x}$ and $\phi_x(x,y) = -\frac{\partial u_{z_1}}{\partial y}$, being ϕ_x and ϕ_y the angles that the normal to the mid-surface makes with the z-axis.

By assuming the angles ϕ_x and ϕ_y to not be equal to the partial derivatives of the transverse displacements with respect to the cross-sectional coordinates, it is possible to include the first-order shear effects. The resulting kinematics is known as the plate model introduced in the works by Reissnerr [38] and Mindlin [39].

$$\begin{aligned} u_x(x,y,z) =& u_{x_1}(x,y) + z\phi_y(x,y) \\ u_y(x,y,z) =& u_{y_1}(x,y) + z\phi_x(x,y) \\ u_z(x,y,z) =& u_{z_1}(x,y) \end{aligned} \tag{6}$$

The Reissnerr-Mindlin plate model does not account for the effects due to thickness stretching and, analogously to TBT, it does not satisfy the stress-free condition at the bottom and top faces of the plate.

In order to accommodate the second-order shear effects, it is now clear that at least a third-order displacement field is needed. The most famous plate theory based on third-order kinematic assumptions is perhaps the Reddy plate model [40], which is not reported here for the sake of brevity. However, like the Vlasov model in Eq. (4), it assumes a cubic expansion of the generalized displacement variables through the thickness of the plate. With the advent of advanced materials and structures, plate theories have been extensively developed in the literature and several higher-order models have been formulated from the second half of the last century. The review of higher-order plate models is out of the scope of the present section, whose aim is to demonstrate that higher-order effects demand for refined expansions and, eventually, for the increase of the degrees of freedom involved in the mechanical kinematics. For a more comprehensive review about plate theories the readers are referred to other works, such as [41, 42].

3 Refined CUF models

As explained in the previous section, classical theories have several limitations. The main point is that, in order to predict higher order effects and overcome the physical inconsistencies, the kinematics should be theoretically enriched with an infinite number of terms (see Washizu [43]). This is obviously not possible from a practical point of view and the theories of structure are generally formulated by truncating the expansion of the primary mechanical variables (along the smallest dimensions of the structure domain) to a given order. Nevertheless, the more the terms in the kinematics, the more the complexity of the formulation and resolution of the problem is. The Carrera Unified Formulation (CUF, see [23, 44]) solves this issues by describing the kinematic field in a unified manner that will be then exploited to derive the governing equations in a compact way. The displacement field of one-dimensional models in CUF framework is, in fact, described as a generic expansion of the generalized

displacements (in the case of displacement-based theories) by arbitrary functions of the cross-section coordinates:

$$\mathbf{u}(x,y,z) = F_\tau(x,z)\mathbf{u}_\tau(y) \quad \tau = 1,2,...,M \tag{7}$$

where $u_\tau(y)$ is the vector of general displacements, M is the number of terms in the expansion, τ denotes summation and $F_\tau(x,z)$ defines the 1D model to be used. In fact, depending on the choice of $F_\tau(x,z)$ functions, different classes of beam theories can be implemented.

In the framework of plate theories, CUF can be formulated in an analogous manner (see [17]).

$$\mathbf{u}(x,y,z) = F_\tau(z)\mathbf{u}_\tau(x,y) \quad \tau = 1,2,...,M \tag{8}$$

In the equation above, the generalized displacements are obviously function of the mid-plane coordinates of the plate and the expansion is conducted in the thickness direction. Again, depending on the choice of the F_τ expanding functions, various theories can be formulated. A few examples are given in the following sections. Attention is mainly devoted to beam modelling, which represents the main subject of this paper.

3.1 Taylor Expansions

Taylor Expansion (TE) beam models make use of a hierarchical 2D polynomial set of the type $x^i z^j$ as $F_\tau(x,z)$. For example, the third-order model, $N = 3$, leads to the following displacement field, where constant, linear, quadratic and cubic functions are used:

$$\begin{aligned}
u_x &= u_{x_1} + x\,u_{x_2} + z\,u_{x_3} + x^2\,u_{x_4} + xz\,u_{x_5} + z^2\,u_{x_6} + x^3\,u_{x_7} + x^2z\,u_{x_8} + xz^2\,u_{x_9} + z^3\,u_{x_{10}} \\
u_y &= u_{y_1} + x\,u_{y_2} + z\,u_{y_3} + x^2\,u_{y_4} + xz\,u_{y_5} + z^2\,u_{y_6} + x^3\,u_{y_7} + x^2z\,u_{y_8} + xz^2\,u_{y_9} + z^3\,u_{y_{10}} \\
u_z &= u_{z_1} + x\,u_{z_2} + z\,u_{z_3} + x^2\,u_{z_4} + xz\,u_{z_5} + z^2\,u_{z_6} + x^3\,u_{z_7} + x^2z\,u_{z_8} + xz^2\,u_{z_9} + z^3\,u_{z_{10}}
\end{aligned} \tag{9}$$

It is important to underline that the kinematic fields of the classical beam theories (see Eqs. (1) and (2)) are particular cases of the first order TE model (N=1), which includes just the constant and the linear terms of Eq. (9). A more detailed description of TE models can be found in [23, 45, 28].

Refined models based on Mclaurin polynomials series have been extensively used in the literature to formulate CUF plate models. A third-order plate model is given below for completeness purpose.

$$\begin{aligned}
u_x &= u_{x_1} + z\,u_{x_2} + z^2\,u_{x_3} + z^3\,u_{x_4} \\
u_y &= u_{y_1} + z\,u_{y_2} + z^2\,u_{y_3} + z^3\,u_{y_4} \\
u_z &= u_{z_1} + z\,u_{z_2} + z^2\,u_{z_3} + z^3\,u_{z_4}
\end{aligned} \tag{10}$$

It should be clear that the Vlasov beam theory (Eq. (4)) and the third-order Reddy plate theory [40] are particular cases of the models described in Eqs. (9) and (10), respectively

3.2 Lagrange Expansions

Lagrange Expansions (LE) beam theories are based on the use Lagrange-type polynomials as generic functions over the cross-section. The cross-section is therefore divided into a number

of local expansion sub-domains, whose polynomial degree depends on the type of Lagrange expansion employed. Three-node linear L3, four-node bilinear L4, nine-node cubic L9, and sixteen-node quartic L16 polynomials can be used to formulate refined beam theories (see Carrera and Petrolo [29]). For example, the interpolation functions of a L9 expansion are defined as:

$$\begin{aligned} F_\tau &= \tfrac{1}{4}(r^2 + r\ r_\tau)(s^2 + s\ s_\tau) \qquad \tau = 1,3,5,7 \\ F_\tau &= \tfrac{1}{2}s_\tau^2(s^2 + s\ s_\tau)(1-r^2) + \tfrac{1}{2}r_\tau^2(r^2 + r\ r_\tau)(1-s^2) \qquad \tau = 2,4,6,8 \\ F_\tau &= (1-r^2)(1-s^2) \qquad \tau = 9 \end{aligned} \tag{11}$$

where r and s vary over the cross-section between -1 and $+1$, and r_τ and s_τ represent the locations of the roots in the natural plane. The kinematic field of the single-L9 beam theory is therefore

$$\begin{aligned} u_x &= F_1\ u_{x_1} + F_2\ u_{x_2} + F_3\ u_{x_3} + ... + F_9\ u_{x_9} \\ u_y &= F_1\ u_{y_1} + F_2\ u_{y_2} + F_3\ u_{y_3} + ... + F_9\ u_{y_9} \\ u_z &= F_1\ u_{z_1} + F_2\ u_{z_2} + F_3\ u_{z_3} + ... + F_9\ u_{z_9} \end{aligned} \tag{12}$$

Refined beam models can be obtained by adopting higher order Lagrange polynomials or by using a combination of Lagrange polynomials on multi-domain cross-sections. More details about Lagrange-class beam models can be found in [46, 29, 45, 28].

Lagrange polynomials have been extensively employed in the formulation of variable kinematics plate and shell theories in a unified framework by Kulikov and his co-workers. The readers are referred to the original papers for more details about 2D models based on Lagrange-type expansions, see for example [47, 48].

3.3 Hierarchical Legendre Expansions

3.3.1 HLE beam theories

HLE (Hierarchical Legendre Expansion) beam models represent the object of the study of the present work. The theoretical basis of the Legendre-like functions that are adopted in this paper were presented by Szabó et al. [34, 35]. In those papers, the authors introduced how to use these polynomials to create sets of finite element shape functions, which will be here applied to develop hierarchical refined structural theories. The one-dimensional Legendre polynomials can be defined in several ways, being the most useful for our purposes the recurrent definition:

$$\begin{aligned} L_0 &= 1 \\ L_1 &= x \\ L_k &= \frac{2k-1}{k} x L_{k-1}(x) - \frac{k-1}{k} L_{k-2}(x), \quad k = 2,3,... \end{aligned} \tag{13}$$

This set of polynomials represents an orthonormal basis, and their roots are identical with integration points of Gauss quadrature rules. They also satisfy the Legendre differential

equation. A set of 1D functions can be defined from these polynomials as:

$$\tilde{L}_1(r) = \frac{1}{2}(1-r) \tag{14}$$

$$\tilde{L}_2(r) = \frac{1}{2}(1+r) \tag{15}$$

$$\tilde{L}_i(r) = \phi_{i-1}(r), \qquad i = 3, 4, ..., p+1 \tag{16}$$

being r the local coordinate in the natural domain [-1, 1], and $\phi_j(r)$:

$$\phi_j(r) = \sqrt{\frac{2j-1}{j}} \int_{-1}^{r} L_{j-1}(x)\, dx, \qquad j = 2, 3, 4, ... \tag{17}$$

The first two functions, i.e. Eqs. (14) and (15), are the *nodal modes* and they correspond to the linear Lagrange 1D polynomials. Equation (16) includes all the *internal modes*. This Legendre-based set of functions maintains the orthogonal properties of the Legendre polynomials, in fact,

$$\int_{-1}^{1} \frac{d\tilde{L}_i}{dr} \frac{d\tilde{L}_j}{dr}\, dx = \delta_{ij}, \quad \text{for } i \geq 3 \text{ and } j \geq 1 \text{ or } i \geq 3 \text{ and } j \geq 1 \tag{18}$$

where δ_{ij} is the Kronecker's delta.

[Figure 1 about here.]

Two-dimensional polynomial expansions can be then defined by extending the above procedure to quadrilateral domains on the beam cross-section. In this case, nodal, edge and internal polynomials are used as interpolation functions over the section. They are all included in Fig. 1 until the 7^{th} order. The vertex modes are four in total, one per vertex, and they vanish at all nodes but one. Secondly, the edge modes vanish for all sides of the domain but one. Finally, the internal modes vanish at all sides, and they are just included from the fourth order expansion and higher.

Vertex expansions The nodal or vertex modes correspond to the first-order, quadrilateral Lagrange polynomials:

$$F_\tau = \frac{1}{4}(1 - r_i r)(1 - s_i s) \qquad \tau = 1, 2, 3, 4 \tag{19}$$

where, as for LE models, r and s vary above the domain between -1 and $+1$, and r_τ and s_τ represent the vertex coordinates in the natural plane. In fact, the same cross-sectional functions were used to develop bilinear, LE beam theories in [29], referred to as L4.

Side expansions The side modes are defined for $p \geq 2$ and they are defined in the natural plane as follows

$$F_\tau(r,s) = \frac{1}{2}(1-s)\phi_p(r) \qquad \tau = 5, 9, 13, 18, ... \tag{20}$$

$$F_\tau(r,s) = \frac{1}{2}(1+r)\phi_p(s) \qquad \tau = 6, 10, 14, 19, ... \tag{21}$$

$$F_\tau(r,s) = \frac{1}{2}(1+s)\phi_p(r) \qquad \tau = 7, 11, 15, 20, ... \tag{22}$$

$$F_\tau(r,s) = \frac{1}{2}(1-r)\phi_p(s) \qquad \tau = 8, 14, 16, 21, ... \tag{23}$$

where p represents the polynomial degree (see Fig. 1). It is possible to note that the above functions are expressed in such a way that they satisfy the side-continuity in multi-domain beam theories.

Internal expansions F_τ internal expansions are built by multiplying 1D internal modes. There are $(p-2)(p-3)/2$ internal polynomials for $p \geq 4$ and they vanish at all the edges of the quadrilateral. As an example, the set of sixth-order polynomials contains 3 internal expansions (see Fig. 1), which are

$$F_{28}(r,s) = \phi_4(r)\phi_2(s) \tag{24}$$

$$F_{29}(r,s) = \phi_3(r)\phi_3(s) \tag{25}$$

$$F_{30}(r,s) = \phi_2(r)\phi_4(s) \tag{26}$$

It is important to note that the hierarchical properties of this model are related to the fact that the set of functions of a particular order contains all the polynomials of the lower degrees. As far as the sixth-order HLE beam model is concerned, for example, the set of functions used to define the kinematic terms of expansion includes the internal polynomials introduced in Eqs. (25), (26) and (26), and all the other internal, side and vertex functions of the same polynomial order and below, i.e $\tau = 1, ..., 30$.

3.3.2 HLE plate theories

Plate theories based on Legendre-like kinematics are formulated by adopting the polynomials in Eqs. (14) to (16) as F_τ thickness functions up to the desired order p:

$$\begin{aligned} u_x &= \tilde{L}_1(z)\ u_{x_1} + \tilde{L}_2(z)\ u_{x_2} + \tilde{L}_i(z)\ u_{x_i} \\ u_y &= \tilde{L}_1(z)\ u_{y_1} + \tilde{L}_2(z)\ u_{y_2} + \tilde{L}_i(z)\ u_{y_i} \\ u_z &= \tilde{L}_1(z)\ u_{z_1} + \tilde{L}_2(z)\ u_{z_2} + \tilde{L}_i(z)\ u_{z_i} \end{aligned} \tag{27}$$

where i denotes a summation and ranges from 3 to $p+1$. It is clear that u_{x_1}, u_{y_1} and u_{z_1} are the displacement components of bottom face of the plate, whereas u_{x_2}, u_{y_2} and u_{z_2} are the displacement components of top face. Within the framework of 2D CUF theories, displacement fields like the one depicted in Eq. (10) have been mainly used for the implementation of layer-wise models for laminated structures (see for example [18, 19, 44]).

4 Finite element formulation

The main advantage of CUF is that it allows to write the governing equations and the related finite element arrays in a compact and unified manner, which is formally an invariant with respect to the F_τ functions. In the sections below, the mathematical derivation of the fundamental nucleus (the invariant) of the stiffness matrix in the case of CUF beam models is provided in detail. Although analogous, the derivation of the stiffness matrix for the plate CUF element is not derived here, but it can be found in [44].

4.1 Geometrical relations and constitutive equations

In this section, the same notation and reference system as defined in Section 2 are adopted. Let the 3D displacement vector be defined as:

$$\mathbf{u}(x,y,z) = \left\{ \begin{array}{c} u_x(x,y,z) \\ u_y(x,y,z) \\ u_z(x,y,z) \end{array} \right\} \tag{28}$$

According to classical elasticity, stress and strain tensors can be organized in six-term vectors with no lack of generality. They read, respectively:

$$\begin{aligned} \boldsymbol{\sigma}^T &= \left\{ \begin{array}{cccccc} \sigma_{yy} & \sigma_{xx} & \sigma_{zz} & \sigma_{xz} & \sigma_{yz} & \sigma_{xy} \end{array} \right\} \\ \boldsymbol{\varepsilon}^T &= \left\{ \begin{array}{cccccc} \varepsilon_{yy} & \varepsilon_{xx} & \varepsilon_{zz} & \varepsilon_{xz} & \varepsilon_{yz} & \varepsilon_{xy} \end{array} \right\} \end{aligned} \tag{29}$$

Regarding to this expression, the geometrical relations between strains and displacements with the compact vectorial notation can be defined as:

$$\boldsymbol{\varepsilon} = \mathbf{D}\,\mathbf{u} \tag{30}$$

where, in the case of small deformations and angles of rotations, $\mathbf{D}$ is the following linear differential operator:

$$\mathbf{D} = \left[\begin{array}{ccc} 0 & \frac{\partial}{\partial y} & 0 \\ \frac{\partial}{\partial x} & 0 & 0 \\ 0 & 0 & \frac{\partial}{\partial z} \\ \frac{\partial}{\partial z} & 0 & \frac{\partial}{\partial x} \\ 0 & \frac{\partial}{\partial z} & \frac{\partial}{\partial y} \\ \frac{\partial}{\partial y} & \frac{\partial}{\partial x} & 0 \end{array} \right] \tag{31}$$

On the other hand, for isotropic materials the relation between stresses and strains is obtained through the well-known Hooke's law:

$$\boldsymbol{\sigma} = \mathbf{C}\,\boldsymbol{\varepsilon} \tag{32}$$

where $\mathbf{C}$ is the isotropic stiffness matrix

$$\mathbf{C} = \left[\begin{array}{cccccc} C_{33} & C_{23} & C_{13} & 0 & 0 & 0 \\ C_{23} & C_{22} & C_{12} & 0 & 0 & 0 \\ C_{13} & C_{12} & C_{11} & 0 & 0 & 0 \\ 0 & 0 & 0 & C_{44} & 0 & 0 \\ 0 & 0 & 0 & 0 & C_{55} & 0 \\ 0 & 0 & 0 & 0 & 0 & C_{66} \end{array} \right] \tag{33}$$

The coefficients of the stiffness matrix depend only on the Young's modulus, E, and the Poisson ratio, ν, and they are:

$$\begin{aligned} C_{11} = C_{22} = C_{33} &= \tfrac{(1-\nu)E}{(1+\nu)(1-2\nu)} \\ C_{12} = C_{13} = C_{23} &= \tfrac{\nu E}{(1+\nu)(1-2\nu)} \\ C_{44} = C_{55} = C_{66} &= \tfrac{E}{2(1+\nu)} \end{aligned} \tag{34}$$

4.2 Interpolation of the generalized displacements

The discretization along the longitudinal axis of the beam is made by means of the finite element method. The generalized displacements are in this way described as functions of the unknown nodal vector, $\mathbf{q}_{\tau i}$, and the 1D shape functions, N_i.

$$\mathbf{u}_\tau(y) = N_i(y)\mathbf{q}_{\tau i}, \qquad i = 1, 2, ..., n_{elem} \tag{35}$$

where n_{elem} is the number of nodes per element and the unknown nodal vector is defined as

$$\mathbf{q}_{\tau i} = \left\{ \begin{array}{ccc} q_{u_{x}\tau i} & q_{u_{y}\tau i} & q_{u_{z}\tau i} \end{array} \right\}^T \tag{36}$$

Different sets of polynomials can be used to define FEM elements. Lagrange interpolating polynomials have been chosen in this work to generate cubic one-dimensional elements. For the sake of brevity, their expression is not provided, but it can be found in the book by Carrera et. al [23], in which two-node (B2), three-node (B3) and four-node (B4) elements are described.

4.3 Fundamental nucleus of the unified beam element

The governing equations are obtained via the principle of virtual displacements. This variational statement sets as a necessary condition for the equilibrium of a structure that the virtual variation of the internal work has to be the same as the virtual variation of the external work, or:

$$\delta L_{\text{int}} = \delta L_{\text{ext}} \tag{37}$$

The internal work is equivalent to the elastic strain energy

$$\delta L_{int} = \int_l \int_\Omega \delta \boldsymbol{\varepsilon}^T \boldsymbol{\sigma} \, d\Omega \, dy \tag{38}$$

where l stands for the length of the beam and Ω is the cross-section domain. By adopting the geometrical relation (Eq. (30)), the constitutive law (Eq. (32)), the CUF kinematic field (Eq. (7)) and the FEM discretization (Eq. (35)), the internal work can be rewritten as:

$$\delta L_{\text{int}} = \delta \mathbf{q}_{\tau i}^T \mathbf{K}^{\tau sij} \mathbf{q}_{sj} \tag{39}$$

where $\boldsymbol{K}^{\tau sij}$ is the 3×3 fundamental nucleus of the stiffness matrix. The nine terms of this matrix are given in the following:

$$
\begin{aligned}
K_{xx}^{\tau sij} &= C_{22}\int_l N_i\,N_j\,\mathrm{d}y\int_\Omega F_{\tau,x}F_{s,x}\,d\Omega + C_{44}\int_l N_i\,N_j\,\mathrm{d}y\int_\Omega F_{\tau,z}F_{s,z}\,d\Omega + \\
&\quad + C_{66}\int_l N_{i,y}\,N_{j,y}\,\mathrm{d}y\int_\Omega F_\tau F_s\,d\Omega \\
K_{xy}^{\tau sij} &= C_{23}\int_l N_i\,N_{j,y}\,\mathrm{d}y\int_\Omega F_\tau F_{s,x}\,d\Omega + C_{66}\int_l N_{i,y}\,N_j\,\mathrm{d}y\int_\Omega F_{\tau,x}F_s\,d\Omega \\
K_{xz}^{\tau sij} &= C_{12}\int_l N_i\,N_j\,\mathrm{d}y\int_\Omega F_{\tau,z}F_{s,x}\,d\Omega + C_{44}\int_l N_i\,N_j\,\mathrm{d}y\int_\Omega F_{\tau,x}F_{s,z}\,d\Omega \\
K_{yx}^{\tau sij} &= C_{23}\int_l N_{i,y}\,N_j\,\mathrm{d}y\int_\Omega F_{\tau,x}F_s\,d\Omega + C_{66}\int_l N_i\,N_{j,y}\,\mathrm{d}y\int_\Omega F_\tau F_{s,x}\,d\Omega \\
K_{yy}^{\tau sij} &= C_{33}\int_l N_{i,y}\,N_{j,y}\,\mathrm{d}y\int_\Omega F_\tau F_s\,d\Omega + C_{55}\int_l N_i\,N_j\,\mathrm{d}y\int_\Omega F_{\tau,z}F_{s,z}\,d\Omega + \\
&\quad + C_{66}\int_l N_i\,N_j\,\mathrm{d}y\int_\Omega F_{\tau,x}F_{s,x}\,d\Omega \\
K_{yz}^{\tau sij} &= C_{13}\int_l N_{i,y}\,N_j\,\mathrm{d}y\int_\Omega F_{\tau,z}F_s\,d\Omega + C_{55}\int_l N_i\,N_{j,y}\,\mathrm{d}y\int_\Omega F_\tau F_{s,z}\,d\Omega \\
K_{zx}^{\tau sij} &= C_{12}\int_l N_i\,N_j\,\mathrm{d}y\int_\Omega F_{\tau,x}F_{s,z}\,d\Omega + C_{44}\int_l N_i\,N_j\,\mathrm{d}y\int_\Omega F_{\tau,z}F_{s,x}\,d\Omega \\
K_{zy}^{\tau sij} &= C_{13}\int_l N_i\,N_{j,y}\,\mathrm{d}y\int_\Omega F_\tau F_{s,z}\,d\Omega + C_{55}\int_l N_{i,y}\,N_j\,\mathrm{d}y\int_\Omega F_{\tau,z}F_s\,d\Omega \\
K_{zz}^{\tau sij} &= C_{11}\int_l N_i\,N_j\,\mathrm{d}y\int_\Omega F_{\tau,z}F_{s,z}\,d\Omega + C_{44}\int_l N_i\,N_j\,\mathrm{d}y\int_\Omega F_{\tau,x}F_{s,x}\,d\Omega + \\
&\quad + C_{55}\int_l N_{i,y}\,N_{j,y}\,\mathrm{d}y\int_\Omega F_\tau F_s\,d\Omega
\end{aligned}
\tag{40}
$$

The derivation of the fundamental nucleus of the loading vector from the virtual variation of the external load is not reported here for the sake of brevity. It can be found in [23].

[Figure 2 about here.]

It should be noted that the formal expressions of the components of the fundamental nucleus of the stiffness matrix are independent on the choice of the cross-sectional functions F_τ, which determine the theory of structure, and shape functions N_i, which determine the numerical accuracy of the FEM approximation (see Fig. 2). This means that any classical to higher-order beam element can be automatically formulated by appropriately expanding the fundamental nuclei according to the indexes τ, s, i, and j.

In this paper, cubic Lagrange-type shape functions are used as N_i, whereas TE, LE and HLE expansions are used to formulate 1D theories of structures. For the sake of clarity, the differences between TE, LE and HLE finite elements are outlined in Fig. 2. These differences are also briefly discussed hereinafter.

Using TE models, the generalized displacement unknowns (displacements and their derivatives) are expanded on the cross-section surface from the reference axis, and the polynomial

order of the model is increased in a hierarchical manner by adding new terms to the kinematic field. On the other hand, LE models are based on local expansions of pure displacement unknowns within each of the sub-domains in which the surface is divided. According to these definitions, HLE performs as a combination of TE and LE. In fact, the unknowns of the HLE models are generalized displacements (displacements and derivatives) as for TE, and the expansion order is also increased in a hierarchical manner. Moreover, Legendre-like expansions can be enriched locally over the physical surface of the cross-section, as for LE models. According to these characteristics, the expansion order is set as a free input of the model that determines the number of unknowns to be solved. At the same time, the kinematic field can be enriched in particular zones of interest through the definition of multi-domain cross-sections.

5 Numerical results

5.1 Square cross-section beam

In order to assess the novel HLE theory, a clamped-free square section beam is considered. The geometry of the cross-section is shown in Fig. 3. The height, h, and the width, b, are both equal to 0.2 m. The slenderness ratio, L/h, is equal to 10, resulting the length equal to 2 m. Ten four-node Lagrange-type B4 elements are employed for the longitudinal mesh, a number that, according to [29], ensure convergent results. Two point loads with magnitude equal to -25 N are applied at the lower corners of the cross-section, in $[\pm b/2, L, -h/2]$. An isotropic Aluminium alloy is employed in all the assessments carried out in this work, being its mechanical characteristics the following: Young modulus, E, equal to 75 GPa and the Poisson ratio, ν, equal to 0.33.

[Figure 3 about here.]

In the first analysis, HLE models are developed by adopting a single quadrilateral domain over the cross-section. The first 8 degrees of the Legendre-like polynomial expansions are accounted for and compared with the results from [29] for the same assessment, in which TE and LE models were used. A solid model has also been created with the commercial software MSC Nastran to serve as a reference for the results. For this and the remaining numerical examples, six-sided Nastran brick elements (CHEXA) have been used to build the reference solid models, which are the results of convergence analyses to ensure fair comparison with the proposed higher-order methodologies. Table 1 shows the number of degrees of freedom, $DOFs$, and the number expansion terms, M, for each model considered.

[Table 1 about here.]

Figure 4 shows the vertical displacement (u_z) distribution along the lower edge of the loaded section for the Solid, L9 and HLE models. The normal stresses, σ_{yy}, and shear stresses, σ_{yz}, are measured along the z-axis at the mid-span section and they are shown in Figs. 5 (a)

and (b), respectively. Table 2 shows the values of these parameters in some representative points of the beam. The displacements at the left bottom vertex of the tip are compared with classic models (EBBT and TBT), TE (from N=1 to N=4 orders) and LE models (see [29]). L9 and Solid solutions are also included for both normal and shear stresses. Two conclusions can be extracted from these results:

- The displacements distribution calculated with HLE models gets closer to the Solid solution as the polynomial order is increased. For instance, the HL8 model is able to account for localized effects due to the point loads. The results obtained with the first expansion order (HL1) are not plotted since this linear-polynomial expansion provides much lower absolute values, having a constant value of $-1,115 \times 10^{-5}$ m along the edge.
- Neither the first two expansion orders of the HLE nor the L9 model are able to represent correctly the shear stresses (σ_{yz}), which should be zero at both free borders according to the stress-free conditions for the edges. Instead, HLE models above the third order provide more accurate values, getting closer to zero as the order increases. It should be noted that the Solid model, whose mesh has not been refined in the vicinities of the free-borders, lacks also in representing correctly the stress-free conditions.

[Figure 4 about here.]

[Figure 5 about here.]

[Table 2 about here.]

In the subsequent assessment, the cross-section domain is divided in several local expansions, as it has been introduced for the development of LE and HLE models. Again, the slenderness ratio, L/h, is equal to 10, the length, L, is 2 m, and the height, h, is 0.2 m. Four different section configurations are studied: single, two (1×2 and 2×1) and four sub-domain distributions (2×2). Figure 6 shows the multi-domain cross-sections used to develop the present beam theories. The same loads as in the previous case are applied at the bottom corners of the tip section. Table 3 shows the vertical displacements, u_z, at one of the loaded points for the different expansion configurations. The results obtained by using Lagrange-class L4 models and the analytical solution calculated by means of the EBBT are also referred here. It is possible to see that the first order HLE model provides the same displacement values as the L4 model, since these models use the same expansion functions. Also, it should be noted that multi-domain models converge faster to the same solution.

[Figure 6 about here.]

[Table 3 about here.]

5.2 Plate structures and comparisons between 1D and 2D models

In this section the performances of the present 1D refined models for the analysis of thin to thick plate structures subjected to various boundary conditions are compared to those of already established 2D CUF theories. The utilized 2D CUF models make use of a 9-node MITC (Mixed Interpolation of Tensorial Components) element to eliminate shear locking, whereas Legendre polynomials are adopted as thickness functions (see Eq. (27)). The sides of the plate under consideration are equal to 1 m and three different thicknesses (h) are considered: 0.1, 0.01 and 0.001 m. The same Aluminium alloy as in the previous assessment ($E = 75$ GPa and $\nu = 0.33$) is employed and a pressure load of $p = 1$ Pa is applied on the upper face of the plate. As far as the 1D models are concerned, 10 B4 elements are used along the beam axis, whereas a mesh of 10×10 MITC elements are adopted for the 2D models. Figure 7 shows the finite element discretization of both 2D and 1D models employed in this section. In particular, Fig. 7b also shows the cross-section of the beam in the xz-plane to readily underline that six domain expansions for the HLE approximation are adopted.

[Figure 7 about here.]

Four different cases of boundary conditions are considered. Namely, plates with two opposite sides clamped, simply-supported on two opposite sides, all the sides clamped, and with simply-supported on all the sides are analysed. Table 4 quotes the results in terms of displacement and stress components for the clamped-clamped case and various thickness-to-side ratio. A fourth-order expansion order along the thickness is considered for the plate model (LD4), whereas fourth- and eight-order polynomial expansions are used in the beam analysis. Tables 5, 6 and 7 show the analogous results for all the other boundary conditions considered. For the sake of completeness, solid Nastran solutions have also been included for $h/a = 0.1$ and 0.01 in the double clamped case (see Table 4). All the solutions are presented in a dimensionless manner by using the following relations:

$$u_z^* = \frac{Eh^3 u_z}{a^4 p} \qquad \sigma_{ii}^* = \frac{h^2 \sigma_{ii}}{a^2 p} \qquad \sigma_{ij}^* = \frac{h\sigma_{ij}}{ap} \tag{41}$$

being a the length of the side, h the thickness, E the Young modulus and p the pressure.

[Table 4 about here.]

[Table 5 about here.]

[Table 6 about here.]

[Table 7 about here.]

It is clear that, due to the refined capabilities of the present HLE and the possibility to apply boundary conditions at any point of the 3D geometry and, thus, on the physical sides laying along the beam axis (which is not possible in conventional beam theories), the proposed refined beam model can be successfully applied to the analysis of plate-like structures. Some further aspects can be observed from the results:

- In terms of displacements, the maximum difference between the HLE beam model and the Nastran solid solutions results is 0.95 % for the case $h/a = 0.1$. The worst performance of the proposed beam model corresponds to the stresses in the transverse direction, σ_{xx}, being 10.08 % and 6.02 % the major differences of the HL4 and HL8 beam models in comparison with the solid solution. However, a remarkable fact is that the HLE models provide shear stresses σ_{yz} that are closer to the 3D solution than the LD4 plate model.

- The maximum relative error in terms of displacements (8.59 %) between plate and beam models occurs for $h/a = 0.1$ and all sides clamped, see Table 6.

- In most cases considered, the fourth-order HLE model provide convergent results. To maintain the accuracy, it would be possible to reduce the number of domain expansions within the cross-section and increase the polynomial order, or reduce the polynomial order and use more domain expansions.

- In the case of symmetric boundary conditions (Tables 6 and 7), the in-plane normal stresses σ_{xx} and σ_{yy} should be equal each other. Obviously, the plate model perfectly satisfy this statement since the finite element space is the same in both x and y directions. On the other hand, the present beam model accomplish fairly good results for this parameters, showing the enhanced capabilities of HLE high-order expansion to capture shell-like solutions.

  This is not perfectly true in the case of HLE, because the finite element approximation along y has a different order with respect to the HLE expansion along the cross-sectional direction x.

5.3 C-section beam

[Figure 8 about here.]

More complex geometries of beams are hereinafter accounted for in order to show the enhanced capabilities of the HLE beam models. A cantilever C-section beam is considered first (see Fig. 8). Its dimensions are the following: height, h, and upper flange width, b_2, are equal to 1 m; lower flange width, b_1, is equal to 0.5 m, with the thickness, t, equal to 0.1 m. The slenderness ratio, L/h, is equal to 20. Regarding LE and HLE models, two different multi-domain cross-sections are considered: (a) 6 and (b) 9 expansion sub-domains (see Fig. 9). Two opposite vertical point forces are applied at $[0, L, \pm 0.4]$: one at the middle of the upper flange and the other one at the edge of the lower one. Its magnitudes are -1 N for the first one and $+1$ N for the lower one. The vertical displacements, u_z, obtained at the upper free edge of the top flange, $[0, L, +0.4]$, are displayed in Table 8. As for the previous assessment, both Taylor-type and Lagrange-type models are also considered, together with

an MSC Nastran solid model. Figure 10 shows a scaled representation of the displacements at the tip. Some remarks can be pointed out from these results:

- Again, LE solutions fall between the second and third expansion order of the HLE, whose values for higher orders result to be in good agreement with the ones obtained with the Nastran solid model.

- On the other hand, the classical model is not capable of representing the effects of this load case, and Taylor-type models result to be not very accurate for the study of this type of problems. For instance, the eleventh-order TE model has more than 15 % of error in comparison with the solid model, being its computational costs even higher than the 6HL4 model, whose error is less than 2 %. The reason is that, as it has been explained before, LE and HLE models make use of localized expansions at the cross-section level, whereas TE are built by expanding the generalized displacements from the beam axis.

[Figure 9 about here.]

[Figure 10 about here.]

[Table 8 about here.]

A second load case is considered for the same C-section beam (see Fig. 8). In this case, a flexural-torsional load case is analysed by using a vertical force of -1 N applied at the lower right corner of the tip, at $[b_1, L, -h/2]$. The vertical displacements, u_z, measured at the edge of the upper flange are displayed in Table 9. The first column shows the different models considered, whereas the second and the third columns include the displacements and the number of degrees of freedom for each model, respectively. The displacement solutions obtained with HLE models converge to the ones obtained with the solid case. Figure 11 shows the normal σ_{yy} (a) and shear σ_{yz} (b) stresses along the web. A 40 B4 mesh along the y-axis has been employed to obtain both stress distributions. This discretization has been chosen on the basis of the convergence analysis shown in Table 10, in which the different solutions are obtained for a increasing number of B4 FEM elements along the longitudinal axis. Out of this study, it is possible to see that the displacement and normal stress solutions, u_z and σ_{yy}, are accurate enough with the minimum number of FEM elements tested. On the other hand, shear stresses, σ_{yz}, measured at the top of the flange, return to values close to zero as the number of FEM elements grows, satisfying the stress-free conditions at the edge. Moreover, the convergence of these solutions depend also on the polynomial order of the model, being necessary to use more beam elements as the expansion order increases. Finally, the tip displacements of the C-section beam under the proposed load condition is shown in Fig. 12.

[Table 9 about here.]

[Figure 11 about here.]

[Table 10 about here.]

[Figure 12 about here.]

5.4 Hollow square cross-section

[Figure 13 about here.]

Let us consider now a hollow square beam whose geometry is shown in Fig. 13. The length-to-height ratio, L/h, is equal to 20, the height-to-thickness ratio, h/t , is equal to 10 with h as high as 1 m, being t equal to 0.1 m and the width, b, is the same as h. The beam is clamped at both ends and a vertical point load of magnitude 1 N is applied at the center of the lower edge at mid-span, at $[0, L/2, h/2]$. Two different cross-section domain configurations are considered for the development of LE and HLE theories: (a) 9 sub-domains, and (b) 11 sub-domains. As shown in Fig. 14, the refinement of the cross-section expansion domain of the second case is concentrated around the loaded point. In this case, 10 B4 elements are used for the longitudinal beam element distribution. The displacements, measured at the loaded point, can be found in Table 11. It includes also other solutions obtained by means of EBBM, TE and LE theories. A solid MSC Nastran model is also used as a reference. Two conclusions come out from this study:

- HLE models result more accurate for the study of thin-walled beams than TE and LE. In fact, the solutions obtained by using high-order HLE models tend to the MSC Nastran Solid value while reducing in great manner the computational costs.

- As expected, the HL2 models show similar behaviour of L9 models when the same cross-section domain configuration is employed, because both HL2 and L9 models employ second order polynomials for the cross-section expansions. The third order model, HL3, is refined enough to overcome the performance of LE models. In fact, as it is clear from the results (see Table 11), the accuracy of the solutions in terms of displacements increases continuously with higher polynomial orders of the expansions.

[Figure 14 about here.]

[Table 11 about here.]

5.5 Open hollow square cross-section

[Figure 15 about here.]

The last example deals with the case of a hollow square beam with a cut. The section is forced to open at the cut, but no flexural loads are applied, so just cross-sectional effects are expected. The cross-section geometry is the same as the hollow square section without cut, shown in Fig. 13. The length-to-height ratio, L/h, is equal to 20. The height-to-thickness ratio, h/t , is equal to 10 with h as high as 1 m, being t equal to 0.1 m. The width, b, is the same as h. Three different cross-section configurations are considered now for the development of multi-domain theories: 9 divisions, 11 divisions with the refinement around the cut, and 11 divisions with the webs divided in 2 sub-domains (see Fig. 15). The beam is clamped at one end and free at the opposite end, where four point loads are applied in correspondence of the cut. Two of them at $[0, L, -0.4]$ with magnitudes of ± 0.5 N and the other two $[0, L, -0.5]$ also with magnitudes of ± 0.5 N. The horizontal displacements, u_x, are measured at the right side of the cut at the lower vertex, and they are displayed in Table 12. Although the three cross-section distributions provide similar results, it is possible to see that the 11HL^b models provide higher values than the other two. This is due to the bending effects that appear on the webs, that can be better represented with 2 expansion sub-domains instead of a single one. Finally, Fig. 16 shows the deformed configuration of the tip section. It is worth mentioning that, for this analysis case, the present HLE models provide displacements results which are larger then those from Nastran solid models if sufficiently higher-order expansions are adopted.

[Table 12 about here.]

[Figure 16 about here.]

6 Conclusions

In this paper, refined beam and plate models have been discussed. Particular attention has been given to a novel refined beam finite element based on the Carrera Unified Formulation (CUF). CUF is an advanced tool that enables to formulate theories of structure in a unified manner. In the case of one-dimensional models, for example, CUF expresses the displacement field as an arbitrary expansion of the generalized unknowns that are functions of the beam axis. The expansion is made by adopting generic functions of the beam cross-section coordinates, F_τ. Depending on the choice of those functions, different beam models can be implemented. For example, TE (Taylor Expansion) models employ Taylor-like polynomials of order N as F_τ, being classical beam theories particular cases of lower-order TE. Lagrange polynomials are, on the other hand, adopted in the case of LE (Lagrange Expansion) models, and they have only pure displacement unknowns.

In the present work, a new class of CUF beam models has been proposed by employing Hierarchical Legendre-like Expansions (HLE). HLE beam models have the advantages of both TE and LE models, but without retaining any of their disadvantages. For example, due to the hierarchy of the cross-sectional functions, the beam theory order is a pure scalar input parameter if HLE or TE are used. On the other hand, increasing the theory order in LE models

requires the re-collocation of the cross-sectional sub-domains. This aspect is of fundamental importance as far as the burden related to the model building and refinement is concerned. Moreover, in HLE as well as in LE approaches, the physical surfaces of the structures are used in the formulation of the mathematical modelling with no geometry approximation loss. Furthermore, HLE methodology allows one to refine the beam model kinematics locally, at the cross-section level. The main advantage of LE models that still is of primary importance is that only pure displacement variables are involved as fundamental unknowns. This aspect may result in a considerable advantage in the formulation of geometrically non-linear formulations, in which rotations and high-order unknowns can be difficult to handle.

Nevertheless, the accuracy of the novel HLE 1D finite beam element has been widely discussed and validated. The enhanced capabilities and the low computational costs of the proposed technique when applied to short, thin-walled and open cross-section beams as well as to plate structures are evident from the analyses conducted. Undoubtedly, HLE results in the best compromise among CUF beam theories as far as accuracy, computational efforts and ease in model building are concerned.

Acknowledgements

This research has been developed in the framework of the FULLCOMP project. The H2020 Marie Skłodowska-Curie European Training Network is gratefully acknowledged.

References

[1] L. Euler. *De curvis elasticis*. Lausanne and Geneva: Bousquet, 1744.

[2] S. P. Timoshenko. On the transverse vibrations of bars of uniform cross section. *Philosophical Magazine*, 43:125–131, 1922.

[3] K. Kapania and S. Raciti. Recent advances in analysis of laminated beams and plates, part I: Shear effects and buckling. *AIAA Journal*, 27(7):923–935, 1989.

[4] K. Kapania and S. Raciti. Recent advances in analysis of laminated beams and plates, part II: Vibrations and wave propagation. *AIAA Journal*, 27(7):935–946, 1989.

[5] J. N. Reddy. On locking-free shear deformable beam finite elements. *Computer methods in applied mechanics and engineerlng*, 149:113–132, 1997.

[6] R. U. Vinayak, G. Prathap, and B. P. Naganarayana. Beam elements based on a higher order theory - I. Formulation and analysis of performance. *Computers and Structures*, 58(4):775–789, 1996.

[7] F. Gruttmann, R. Sauer, and W. Wagner. Shear stresses in prismatic beams with arbitrary cross-sections. *International Journal for Numerical Methods in Engineering*, 45:865–889, 1999.

[8] W. Wagner and F. Gruttmann. A displacement method for the analysis of flexural shear stresses in thin-walled isotropic composite beams. *Computers and Structures*, 80:1843–1851, 2002.

[9] J. Petrolito. Siffness analysis of beams using a higher-order theory. *Computers and Structures*, 55(1):33–39, 1995.

[10] M. Eisenberger. An exact high order beam element. *Computers and Structures*, 81:147–152, 2003.

[11] N. Silvestre. Generalised beam theory to analyse the buckling behaviour of circular cylindrical shells and tubes. *Thin-Walled Structures*, 45:185–198, 2007.

[12] S. Rendek and I. Baláž. Distortion of thin-walled beams. *Thin-Walled Structures*, 42:255–277, 2004.

[13] S. de Miranda, A. Madeo, R. Miletta, and F. Ubertini. On the relationship of the shear deformable generalized beam theory with classical and non-classical theories. *International Journal of Solids and Structures*, 51(2122):3698–3709, 2014.

[14] Q. Cao, M. Ding, X. Jiang, J. Ju, H. Wang, and P. Zhang. Element for beam dynamic analysis based on analytical deflection trial function. *Mathematical Problems in Engineering*, 2015:art. no 582326 1–10, 2015.

[15] A. Genoese, A. Genoese, A. Bilotta, and G. Garcea. A mixed beam model with non-uniform warpings derived from the saint vennt rod. *Computers and Structures*, 121:87–98, 2013.

[16] E. Carrera. Theories and finite elements for multilayered, anisotropic, composite plates and shells. *Archives of Computational Methods in Engineering*, 9(2):87–140, 2002.

[17] E. Carrera. Theories and finite elements for multilayered plates and shells: a unified compact formulation with numerical assessment and benchmarking. *Archives of Computational Methods in Engineering*, 10(3):216–296, 2003.

[18] M. Cinefra, S. Valvano, and E. Carrera. A layer-wise MITC9 finite element for the free-vibration analysis of plates with piezo-patches. *International Journal of Smart and Nano Materials*, 6(2):85–104, 2015.

[19] A. Pagani, S. Valvano, and E. Carrera. Analysis of laminated composites and sandwich structures by variable-kinematic MITC9 plate elements. *Journal of Sandwich Structures and Materials*, 2016. In Press.

[20] L. Dozio. Natural frequencies of sandwich plates with FGM core via variable-kinematic 2-d ritz models. *Composite Structures*, 96:561–568, 2013.

[21] M. D'Ottavio, P. Vidal, E. Valot, and O. Polit. Assessment of plate theories for free-edge effects. *Composites Part B: Engineering*, 48:111–121, 2013.

[22] E. Carrera and G. Giunta. Refined beam theories based on Carrera's unified formulation. *International Journal of Applied Mechanics*, 2(1):117–143, 2010.

[23] M. Petrolo E. Carrera, G. Giunta. *Beam structures: classical and advanced theories*. John Wiley and Sons, 2011.

[24] E. Carrera, M. Petrolo, and E. Zappino. Performance of cuf approach to analyze the structural behavior of slender bodies. *Journal of Structural Engineering*, 138(2):285–297, 2012.

[25] E. Carrera, A. Pagani, and M. Petrolo. Use of Lagrange multipliers to combine 1D variable kinematic finite elements. *Computers and Structures*, 129:194–206, 2013.

[26] E. Carrera and A. Pagani. Analysis of reinforced and thin-walled structures by multi-line refined 1D/beam models. *International Journal of Mechanical Sciences*, 75:278–287, 2013.

[27] E. Carrera and A. Pagani. Evaluation of the accuracy of classical beam FE models via locking-free hierarchically refined elements. *International Journal of Mechanical Sciences*, 100:169–179, 2015.

[28] E. Carrera, A. Pagani, M. Petrolo, and E. Zappino. Recent developments on refined theories for beams with applications. *Mechanical Engineering Reviews*, 2(2):14–00298, 2015.

[29] E. Carrera and M. Petrolo. Refined beam elements with only displacement variables and plate/shell capabilities. *Meccanica*, 47(3):537–556, 2012.

[30] E. Carrera, M. Maiarú, and M. Petrolo. Component-wise analysis of laminated anisotropic composites. *International Journal of Solids and Structures*, 49:1839–1851, 2012.

[31] E. Carrera, A. Pagani, and M. Petrolo. Classical, refined and component-wise theories for static analysis of reinforced-shell wing structures. *AIAA Journal*, 51(5):1255–1268, 2013.

[32] E. Carrera, A. Pagani, and M. Petrolo. Refined 1D finite elements for the analysis of secondary, primary, and complete civil engineering structures. *Journal of Structural Engineering*, 141(4):art. no. 04014123, 2014.

[33] I. Babuška, B. A. Szabó, and I. N. Katz. The p-version of the finite element method. *SIAM Journal on Numerical Analysis*, 18(3):515–545, 1981.

[34] B. Szabó, A. Düster, and E. Rank. *The p-Version of the Finite Element Method*. John Wiley and Sons, Ltd, 2004.

[35] B. Szabó and I. Babu˘ka. *Finite Element Spaces*, pages 145–165. John Wiley and Sons, Ltd, 2011.

[36] V.Z. Vlasov. *Thin-walled elastic beams*. National Technical Information Service, 1984.

[37] S. P. Timoshenko and S. Woinowsky-Krieger. *Theory of plates and shells*. McGraw-Hill, 1959.

[38] E. Reissner. The effect of transverse shear deformation on the bending of elastic plates. *Journal of Applied Mechanics*, 12(2):69–77, 1945.

[39] R.D. Mindlin. Influence of rotary inertia and shear flexural motion of isotropic, elastic plates. *Journal of Applied Mechanics*, 18:31–38, 1951.

[40] J.N. Reddy. A simple higher–order theory for laminated composites. *Journal of Applied Mechanics*, 51:745–752, 1984.

[41] V. Panc. *Theories of Elastic Plates*. Noordhoff International Publishing, 1975.

[42] Y.M. Ghugal and R.P. Shimpi. A review of refined shear deformation theories of isotropic and anisotropic laminated plates. *Journal of Reinforced Plastics and Composites*, 21(9):775–813, 2002.

[43] K. Washizu. *Variational Methods in Elasticity and Plasticity*. Elsevier Science & Technology, 1974.

[44] E. Carrera, M. Cinefra, M. Petrolo, and E. Zappino. *Finite Element Analysis of Structures through Unified Formulation*. John Wiley & Sons, 2014.

[45] E. Carrera and A. Pagani. Free vibration analysis of civil engineering structures by component-wise models. *Journal of Sound and Vibration*, 333(19):4597–4620, 2014.

[46] E. Carrera, A. Pagani, and M. Petrolo. Component-wise method applied to vibration of wing structures. *Journal of Applied Mechanics*, 80(4):art. no. 041012 1–15, 2013.

[47] G.M. Kulikov, A.A. Mamontov, S.V. Plotnikova, and S.A. Mamontov. Exact geometry solid-shell element based on a sampling surfaces technique for 3d stress analysis of doubly-curved composite shells. *Curved and Layered Structures*, 3(1), 2016.

[48] G.M. Kulikov and S.V. Plotnikova. A method of solving three-dimensional problems of elasticity for laminated composite plates. *Mechanics of Composite Materials*, 48(1):15–26, 2012.

List of Figures

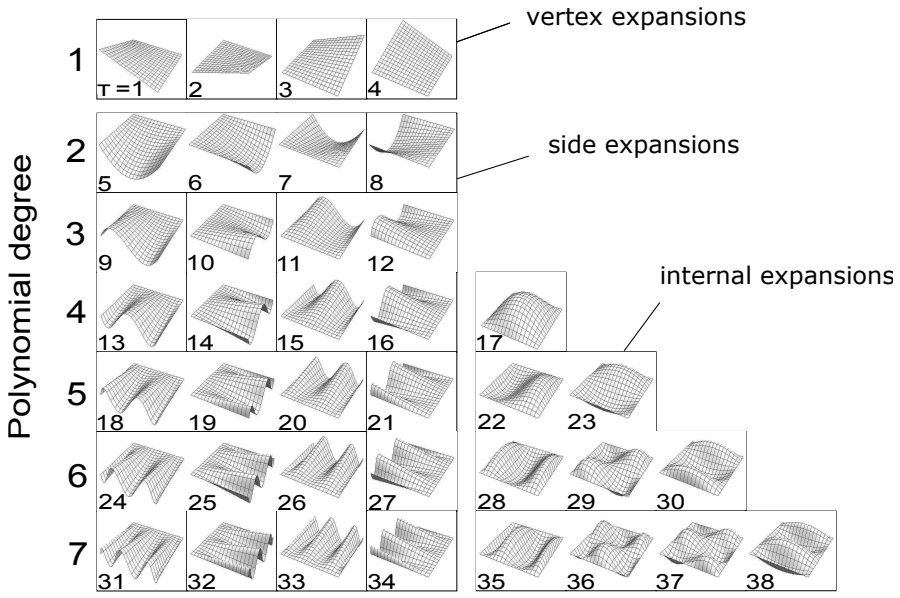

Figure 1: Linear to seventh-order, hierarchical Legendre-type F_τ expansion used for HLE models.

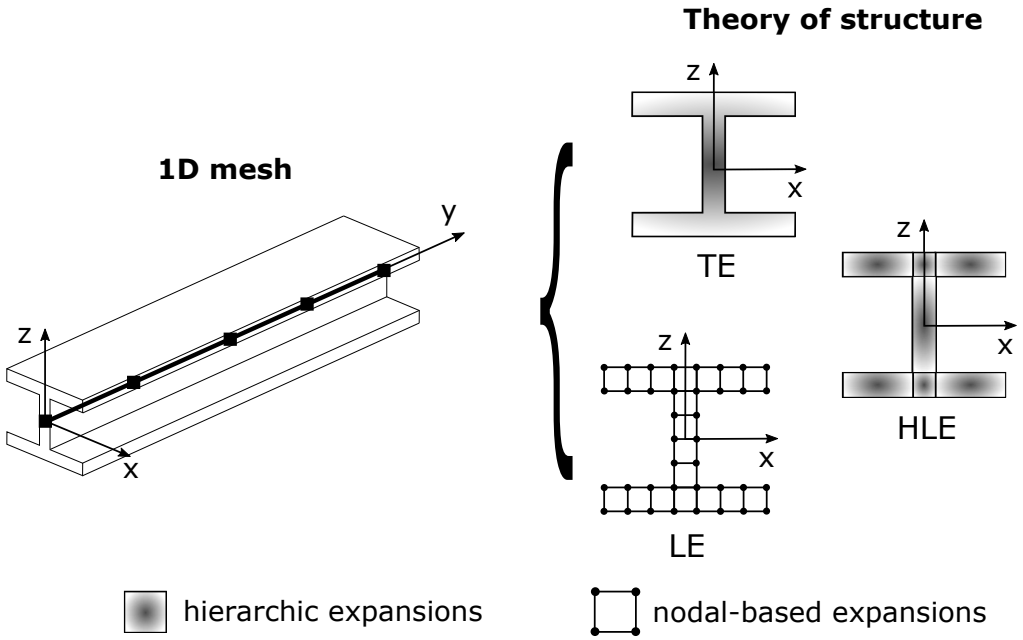

Figure 2: Differences between various refined 1D CUF finite elements

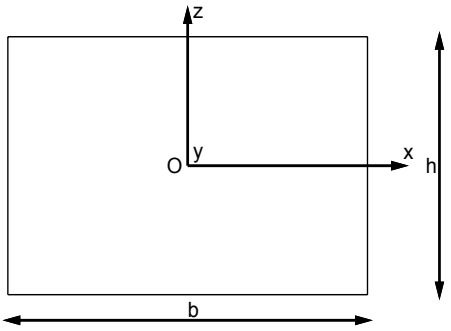

Figure 3: Rectangular cross-section.

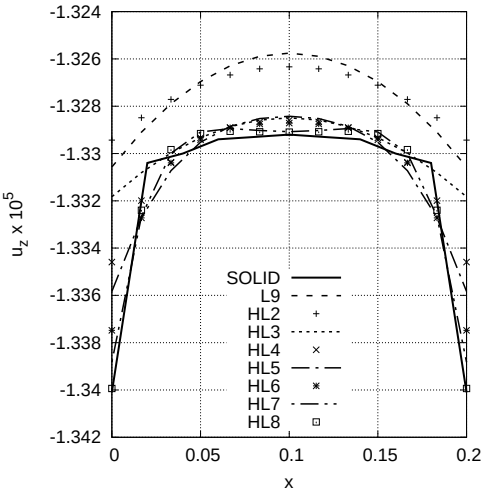

Figure 4: Vertical displacement, u_z, at $[:, L, -h/2]$.

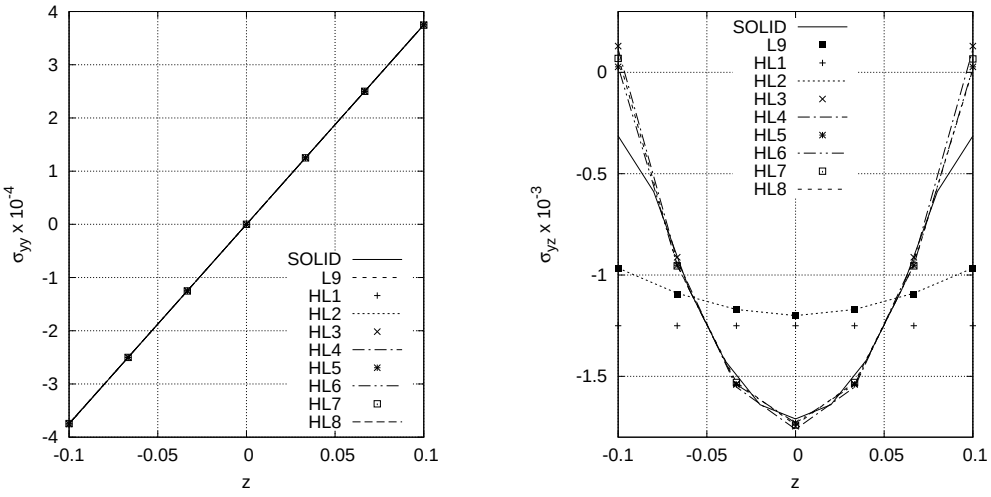

(a) σ_{yy} (b) σ_{yz}

Figure 5: Normal, σ_{yy}, and shear, σ_{yz}, stresses at $[0, L/2, :]$.

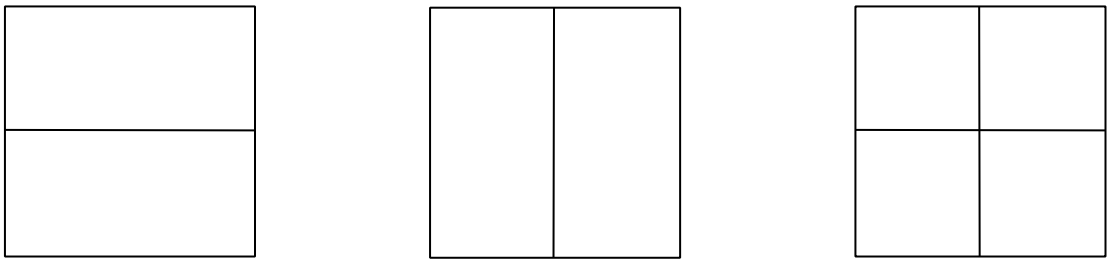

(a) 1×2 sub-domains (b) 2×1 sub-domains (c) 2×2 sub-domains

Figure 6: Cross-section expansion domains for the square beam.

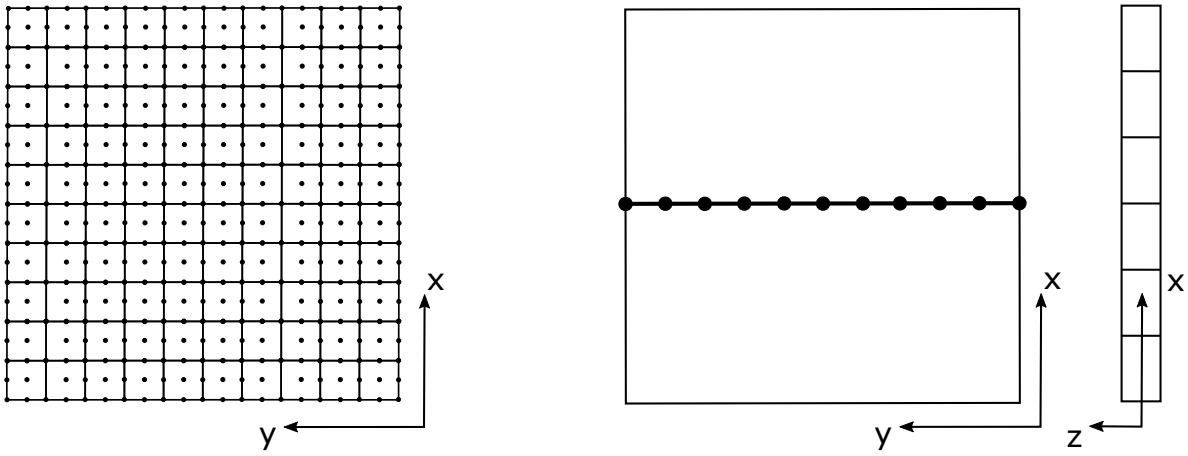

(a) 2D CUF models (b) 1D HLE

Figure 7: Finite element discretizations of the 2D and 1D models of the plate structure.

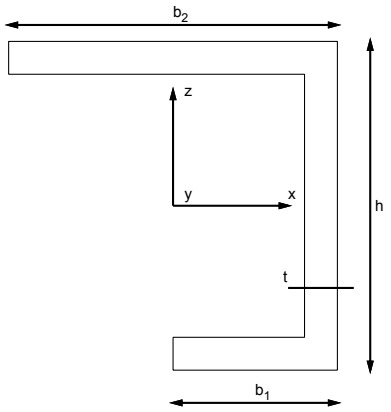

Figure 8: C-shape cross-section.

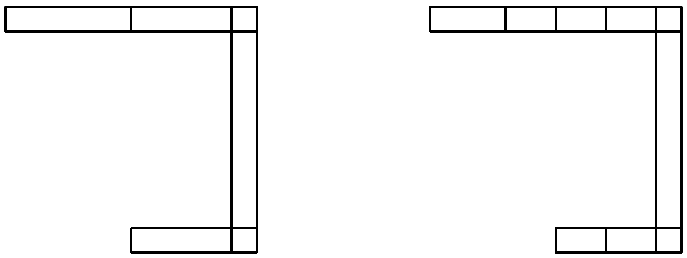

(a) 6 sub-domains (b) 9 sub-domains

Figure 9: Cross-section domain distributions for the C-section beam.

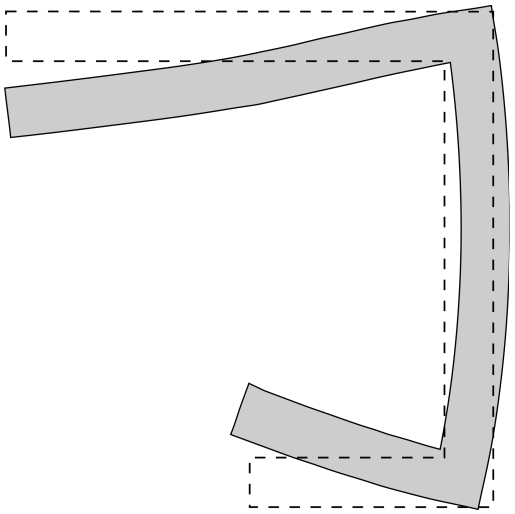

Figure 10: Displacements at the tip of the C-section beam for the 9HL8 model.

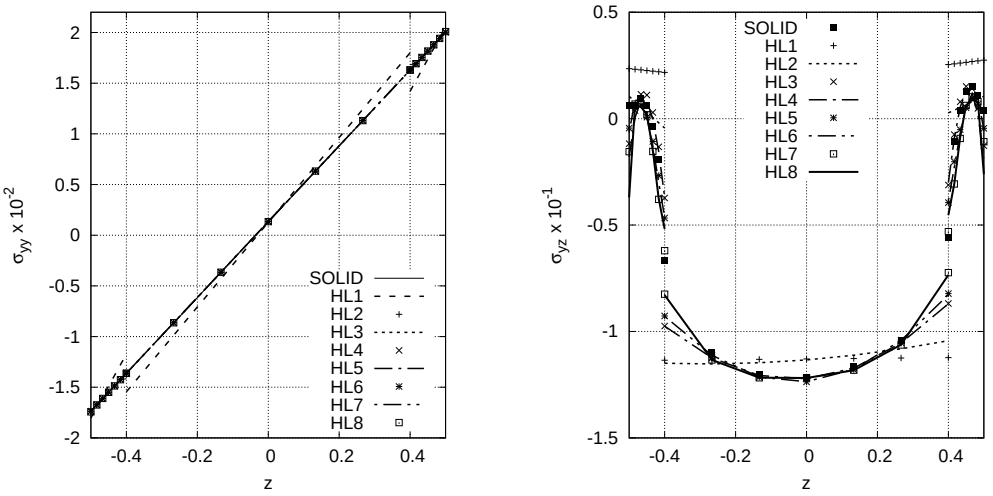

(a) σ_{yy} (b) σ_{yz}

Figure 11: Normal, σ_{yy}, and shear, σ_{yz}, stresses of the C-section beam under flexural-torsional load at $[0.45, L/2, :]$.

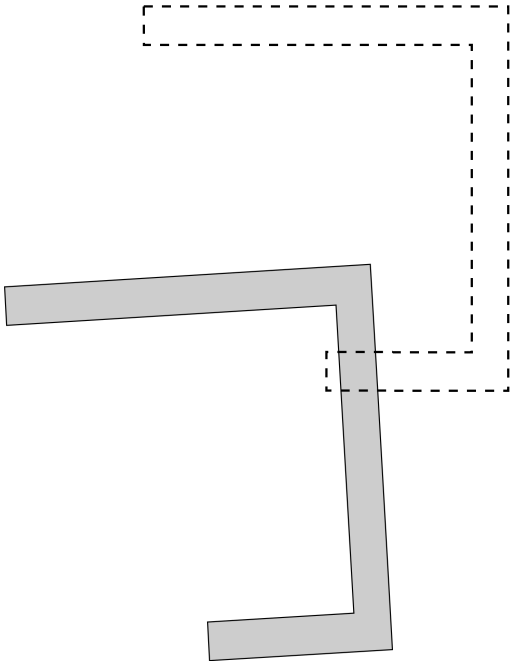

Figure 12: Displacements at the tip of the C-section beam under flexural-torsional loads for the 9HL8 model.

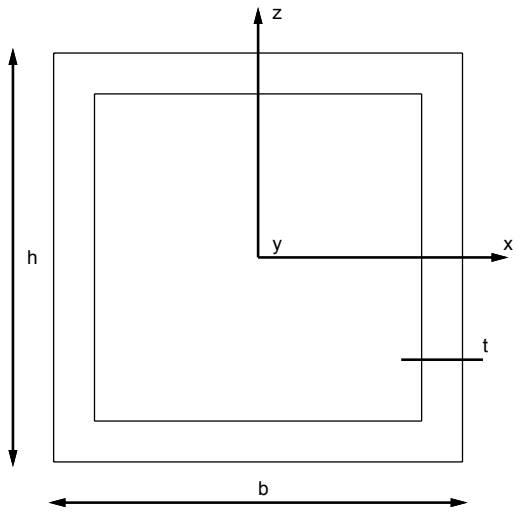

Figure 13: Hollow square cross-section.

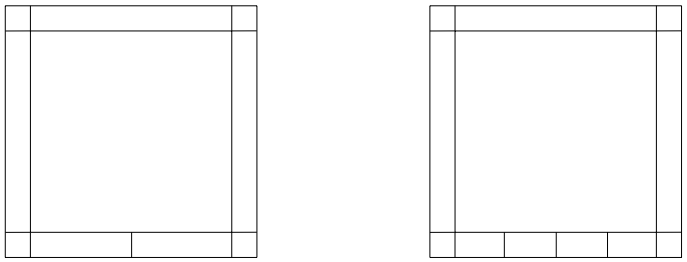

(a) 9 sub-domains (b) 11 sub-domains

Figure 14: Cross-section expansion domains for the hollow square beam.

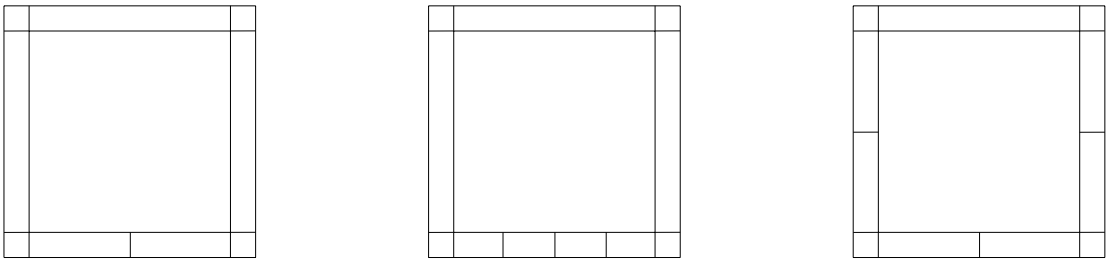

(a) 9 sub-domains (b) 11^a sub-domains(a) (c) 11^b sub-domains

Figure 15: Cross-section domain distributions for the open hollow square beam.

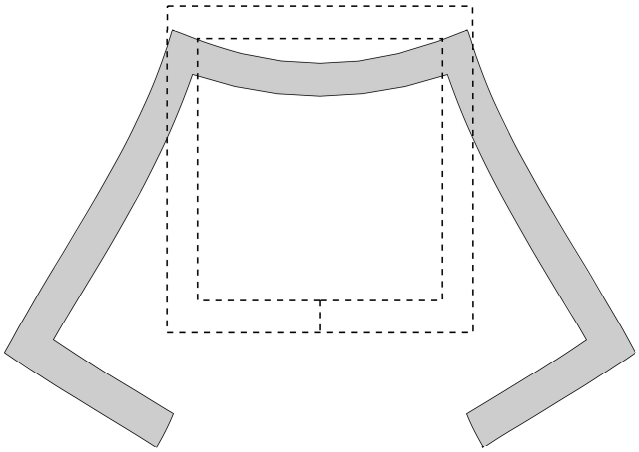

Figure 16: Displacements at the tip of the hollow opened beam for the 11HL8^b model.

List of Tables

model	*DOFs*	*M*
SOLID [29]	18150	–
TE models [29]		
N=1	279	3
N=2	558	6
N=3	930	10
N=4	1395	15
LE models [29]		
L4	372	4
L9	837	9
present HLE models		
HL1	372	4
HL2	744	8
HL3	1116	12
HL4	1581	17
HL5	2139	23
HL6	2790	30
HL7	3534	38
HL8	4371	47

Table 1: Degrees of freedom for each model of the square cross-section beam.

model	$u_z \times 10^5$ $[-b/2, L, -h/2]$	$\sigma_{yy} \times 10^{-4}$ $[0, L/2, h/2]$	$\sigma_{yz} \times 10^{-3}$ $[0, L/2, 0]$
	$u_z \times 10^5$, $u_{z_b} \times 10^5 = -1.333$		
SOLID[29]	-1.340	3.750	-1.708
Classical and refined models based on TE [29]			
EBBT	-1.333	-	-
TBT	-1.343	-	-
N=1	-1.343	-	-
N=2	-1.327	-	-
N=3	-1.329	-	-
N=4	-1.330	-	-
LE models			
L4[29]	-1.115	-	-
L9	-1.331	3.750	-1.198
present HLE models			
HL1	-1.115	3.750	-1.250
HL2	-1.329	3.750	-1.198
HL3	-1.332	3.750	-1.746
HL4	-1.335	3.750	-1.761
HL5	-1.336	3.750	-1.734
HL6	-1.337	3.751	-1.734
HL7	-1.339	3.743	-1.741
HL8	-1.340	3.745	-1.738

Table 2: Displacements and stresses of the square beam ($L/h = 10$).

model	1 sub-domain	1×2 sub-domains	2×1 sub-domains	2×2 sub-domains
		$u_z \times 10^5$, $u_{z_b} \times 10^5 = -1.333$		
L4[29]	-1.115	-1.229	-1.160	-1.262
HL1	-1.115	-1.229	-1.160	-1.262
HL2	-1.329	-1.324	-1.324	-1.324
HL3	-1.332	-1.323	-1.324	-1.324
HL4	-1.335	-1.323	-1.324	-1.324
HL5	-1.336	-1.323	-1.324	-1.324
HL6	-1.337	-1.323	-1.324	-1.324
HL7	-1.339	-1.324	-1.324	-1.324
HL8	-1.340	-1.324	-1.324	-1.324

Table 3: Vertical displacement, $u_z \times 10^5$, for different cross-section domain configurations.

Model	h/a	Expansion	$u_z^* \times 10^2$ [0.5,0.5,h/2]	$\sigma_{xx}^* \times 10^2$ [0.5,0.5,h/2]	$\sigma_{yy}^* \times 10$ [0.5,0.5,h/2]	$\sigma_{yz}^* \times 10$ [0.5,0.25,0.0]	DOFs
Solid	0.1	-	3.060	7.108	2.471	3.574	329967
Plate		LD4	3.022	7.297	2.507	4.962	6615
Beam		6HL4	3.050	6.391	2.401	3.625	7161
		6HL8	3.052	7.536	2.464	3.641	22041
Solid	0.01	-	2.728	7.132	2.424	3.578	742467
Plate		LD4	2.669	7.281	2.449	5.073	6615
Beam		6HL4	2.702	6.778	2.405	3.699	7161
		6HL8	2.702	6.842	2.403	3.697	22041
Plate	0.001	LD4	2.665	7.285	2.448	5.072	6615
Beam		6HL4	2.698	6.502	2.392	3.725	7161
		6HL8	2.698	6.833	2.403	3.727	22041

Table 4: Displacement and stress components of the plate clamped at two opposite sides.

Model	h/a	Expansion	$u_z^* \times 10$ [0.5,0.5,h/2]	$\sigma_{xx}^* \times 10$ [0.5,0.5,h/2]	$\sigma_{yy}^* \times 10$ [0.5,0.5,h/2]	$\sigma_{yz}^* \times 10$ [0.5,0.25,0.0]	DOFs
Plate	0.1	LD4	1.438	1.724	7.421	4.743	6615
Beam		6HL4	1.435	1.625	7.284	3.335	7161
		6HL8	1.435	1.737	7.347	3.355	22041
Plate	0.01	LD4	1.409	1.795	7.401	4.812	6615
Beam		6HL4	1.406	1.660	7.301	3.367	7161
		6HL8	1.406	1.693	7.312	3.385	22041
Plate	0.001	LD4	1.408	1.797	7.401	4.822	6615
Beam		6HL4	1.406	1.710	7.318	3.380	7161
		6HL8	1.406	1.744	7.329	3.400	22041

Table 5: Displacement and stress components of the plate simply-supported at two opposite sides.

Model	h/a	Expansion	$u_z^* \times 10^2$ [0.5,0.5,h/2]	$\sigma_{xx}^* \times 10$ [0.5,0.5,h/2]	$\sigma_{yy}^* \times 10$ [0.5,0.5,h/2]	$\sigma_{yz}^* \times 10$ [0.5,0.25,0.0]	DOFs
Plate	0.1	LD4	1.560	1.486	1.486	3.500	6615
Beam		6HL4	1.571	1.401	1.419	2.249	7161
		6HL8	1.694	1.534	1.568	2.386	22041
Plate	0.01	LD4	1.322	1.406	1.406	3.651	6615
Beam		6HL4	1.342	1.271	1.360	2.330	7161
		6HL8	1.347	1.310	1.376	2.306	22041
Plate	0.001	LD4	1.320	1.404	1.404	3.661	6615
Beam		6HL4	1.340	1.323	1.377	2.343	7161
		6HL8	1.340	1.359	1.389	2.315	22041

Table 6: Displacement and stress components of the plate clamped at all the sides.

Model	h/a	Expansion	$u_z^* \times 10^2$ [0.5,0.5,h/2]	$\sigma_{xx}^* \times 10$ [0.5,0.5,h/2]	$\sigma_{yy}^* \times 10$ [0.5,0.5,h/2]	$\sigma_{yz}^* \times 10$ [0.5,0.25,0.0]	DOFs
Plate	0.1	LD4	4.505	2.980	2.980	3.096	6615
Beam		6HL4	4.894	3.059	3.084	2.081	7161
		6HL8	4.932	3.172	3.170	2.053	22041
Plate	0.01	LD4	4.346	2.950	2.950	3.104	6615
Beam		6HL4	4.392	2.835	2.926	2.105	7161
		6HL8	4.402	2.876	2.943	2.074	22041
Plate	0.001	LD4	4.344	2.950	2.950	3.104	6615
Beam		6HL4	4.362	2.875	2.927	2.083	7161
		6HL8	4.363	2.909	2.939	2.048	22041

Table 7: Displacement and stress components of the plate simply-supported on all the sides.

model	$u_z \times 10^8$ m	DOF
SOLID[29]	−3.067	84600
Classical and refined models based on TE [29]		
EBBM	0.0	155
N=4	−0.245	1395
N=8	−2.161	4185
N=11	−2.565	7254
LE models [29]		
6L9	−2.930	3627
9L9	−2.982	5301
present HLE models		
6HL1	−0.888	1302
6HL2	−2.897	3069
6HL3	−2.963	4836
6HL4	−3.007	7161
6HL5	−3.033	10044
6HL6	−3.057	13485
6HL7	−3.067	17484
6HL8	−3.079	22041
9HL1	−1.071	1860
9HL2	−2.952	4469
9HL3	−2.984	7068
9HL4	−3.029	10509
9HL5	−3.047	14787
9HL6	−3.068	19902
9HL7	−3.075	25854
9HL8	−3.084	32643

Table 8: Vertical displacement, u_z, at the upper free edge of the C-section beam, $[0, L, 0.4]$.

model	$u_z \times 10^6$ m	DOF
SOLID[29]	-1.467	84600
9L9 [29]	-1.457	5301
9HL1	-1.419	1860
9HL2	-1.457	4464
9HL3	-1.459	7068
9HL4	-1.460	10509
9HL5	-1.461	14787
9HL6	-1.461	19902
9HL7	-1.461	25854
9HL8	-1.461	32643

Table 9: Displacements, u_z, of the C-section beam under flexural-torsional load at $[-b_2/2, L, +h/2]$.

model	n elements	$u_z \times 10^6$ m $[-b_2/2, L, h/2]$	$\sigma_{yy} \times 10^{-2}$ Pa $[0.45, L/2, h/2]$	$\sigma_{yz} \times 10^{-1}$ Pa $[0.45, L/2, 0]$	$\sigma_{yz} \times 10^{-1}$ Pa $[0.45, L/2, h/2]$
9HL2	10	-1.457	1.998	-1.117	0.464
	20	-1.462	2.004	-1.133	0.104
	30	-1.463	2.004	-1.133	0.105
	40	-1.463	2.004	-1.133	0.105
9HL5	10	-1.460	1.956	-1.240	2.951
	20	-1.465	2.025	-1.236	-0.944
	30	-1.466	2.001	-1.236	0.044
	40	-1.467	2.004	-1.236	-0.045
9HL8	10	-1.461	1.956	-1.224	3.936
	20	-1.466	2.043	-1.218	-3.325
	30	-1.467	1.985	-1.218	1.298
	40	-1.468	2.009	-1.218	-0.260

Table 10: Various solutions of displacements and stresses for different numbers of beam elements.

model	$u_z \times 10^8$ m	DOF
SOLID[29]	1.374	128952
Classical and refined models based on TE [29]		
EBBM	1.129	155
N=4	1.209	1395
N=8	1.291	4185
N=11	1.309	7254
LE models [29]		
8L9	1.277	4464
9L9	1.308	5022
11L9	1.326	6138
present HLE models		
9HL1	1.210	1674
9HL2	1.307	4185
9HL3	1.337	6696
9HL4	1.340	10044
9HL5	1.348	14229
9HL6	1.345	19251
9HL7	1.347	25110
9HL8	1.348	31806
11HL1	1.231	2046
11HL2	1.324	5115
11HL3	1.340	8184
11HL4	1.343	12276
11HL5	1.345	17391
11HL6	1.347	23529
11HL7	1.348	30690
11HL8	1.349	38874

Table 11: Vertical displacement, u_z, at the loaded point of the hollow cross-section square beam.

model	$u_x \times 10^8$ m	DOF
SOLID[29]	5.292	131400
LE models [29]		
9 L9	4.884	5301
$11L9^a$	4.888	6417
$11L9^b$	5.116	6417
present HLE models		
$9HL1$	1.002	1860
$9HL2$	4.838	4464
$9HL3$	5.123	7068
$9HL4$	5.214	10509
$9HL5$	5.260	14787
$9HL6$	5.304	19902
$9HL7$	5.329	25854
$9HL8$	5.375	32643
$11HL1^a$	1.011	2232
$11HL2^a$	4.851	5394
$11HL3^a$	5.133	8556
$11HL4^a$	5.223	12741
$11HL5^a$	5.267	17949
$11HL6^a$	5.309	24180
$11HL7^a$	5.332	31434
$11HL8^a$	5.355	39711
$11HL1^b$	1.305	2232
$11HL2^b$	5.061	5394
$11HL3^b$	5.154	8556
$11HL4^b$	5.244	12741
$11HL5^b$	5.285	17949
$11HL6^b$	5.327	24180
$11HL7^b$	5.345	31434
$11HL8^b$	5.364	39711

Table 12: Horizontal displacement, u_x, at $[0, L, -h/2]$ of the open hollow square beam.